PLEASE CITE THIS ARTICLE AS DOI: 10.1063/5.0219431

Infrared Signature of the Hydroperoxyalkyl Intermediate (•QOOH) in Cyclohexane Oxidation: An Isomer-Resolved Spectroscopic Study

Tarun Kumar Roy^a, Yujie Qian^a, Christopher A. Sojdak^a, Marisa C. Kozlowski^a, Stephen J. Klippenstein^b and Marsha I. Lester^{a,*}

^a Department of Chemistry, University of Pennsylvania, Philadelphia, PA 19103-6323 USA ^b Chemical Sciences and Engineering Division, Argonne National Laboratory, Lemont, IL 60439, **USA**

Abstract

Infrared (IR) action spectroscopy is utilized to characterize carbon-centered hydroperoxy-cyclohexyl radicals (•QOOH) transiently formed in cyclohexane oxidation. The oxidation pathway leads to three nearly degenerate •QOOH isomers, β -, γ -, and δ -QOOH, which are generated in the laboratory by H-atom abstraction from corresponding ring sites of the cyclohexyl hydroperoxide (CHHP) precursor. IR spectral features of jet-cooled and stabilized •QOOH radicals are observed from 3590 to 7010 cm⁻¹ (ca. 10-20 kcal mol⁻¹) at energies in the vicinity of the transition state (TS) barrier leading to OH radicals that are detected by ultraviolet (UV) laser-induced fluorescence. The experimental approach affords selective detection of β -QOOH, arising from its significantly lower TS barrier to OH products compared to γ and δ isomers, which results in rapid unimolecular decay and near unity branching to OH products. The observed IR spectrum of β-QOOH includes fundamental and overtone OH stretch transitions, overtone CH stretch transitions, and combination bands involving OH or CH stretch with lower frequency modes. Assignment of β-QOOH spectral features is guided by anharmonic frequencies and intensities computed using second-order vibrational perturbation theory. The overtone OH stretch ($2v_{OH}$) of β -QOOH is shifted only a few wavenumbers from that observed for the CHHP precursor, yet they are readily distinguished by their prompt vs. slow dissociation rates to OH products.

^{*} Corresponding author email: <u>milester@sas.upenn.edu</u>

PLEASE CITE THIS ARTICLE AS DOI: 10.1063/5.0219431

Introduction

Cycloalkane oxidation has garnered significant attention in recent years, driven by the growing interest in kinetic modeling of the combustion of conventional and unconventional transportation fuels. Cycloalkanes account for a significant portion (15–40%) of conventional transportation fuels, ¹⁻³ while they are the main component in unconventional transportation fuels such as biomass, coal fuels, and oil sand fuels (up to 100%). 4-6 Yet, cycloalkanes exhibit less efficient low-temperature oxidation than similar size acyclic alkanes. Cycloalkanes are increasingly important as a component of Sustainable Aviation Fuels (SAFs), enabling reduction in the aromatic content of aviation fuels that have a high propensity to produce soot during combustion.⁸ Atmospheric emission and subsequent processing of cycloalkanes via oxidation reactions can also lead to formation of secondary organic aerosols (SOAs). 9-11 Prior studies have shown that SOA yields resulting from oxidation of cycloalkanes are higher than those of acyclic alkanes with equivalent carbon numbers. 12, 13 Indeed, a recent study showed that SOAs formation in an urban area was elevated from ca. 20% to nearly 50% by taking cycloalkanes into account, illustrating the significant role of cycloalkanes in atmospheric SOA formation. ¹³

Cyclohexane is frequently utilized as a model cycloalkane system due to its simplicity and abundance, resulting in many studies of its low-temperature combustion¹⁴ and atmospheric^{15, 16} oxidation processes. Prior experimental studies focused on product characterization as a function of temperature and pressure, in some cases measuring the time-dependent appearance of OH and/or HO₂ products. ¹⁷⁻¹⁹ Recently, the low temperature oxidation chemistry of cyclohexane was studied in a jet-stirred reactor using photoionization mass spectrometry to investigate the intermediates and products. ²⁰ Prior theoretical studies of cyclohexane oxidation have provided the basis for development of kinetic models designed to reproduce a wide range of experimental observations. 19, 21, 22 Recent studies have utilized electronic structure calculations and master equation-based kinetic modeling to investigate the reaction pathways of cyclohexane oxidation. 23, 24

The oxidation of alkane molecules (RH) in the atmosphere and low-temperature (< 1000 K) combustion of hydrocarbon fuels occur via a series of radical reactions. 25-27 These reactions are primarily initiated by OH radicals through H-atom abstraction from an alkyl group to form an alkyl radical (R•) that rapidly reacts with O₂ to generate alkyl peroxy radicals (ROO•). Intramolecular hydrogen abstraction (Hshift) of ROO• can result in the formation of transient carbon-centered hydroperoxyalkyl radical intermediates, which are commonly known as •OOOH. 26 The •OOOH radical consists of a hydroperoxide group (-OOH) and a new alkyl radical center (•Q). •QOOH intermediates can undergo subsequent unimolecular reactions: isomerization back to ROO•, dissociation to OH radicals and cyclic ether products (chain propagation), or direct HO₂ elimination to alkene products. The unimolecular decay pathways of •QOOH typically compete against its bimolecular reaction with O₂ that forms oxygen-

PLEASE CITE THIS ARTICLE AS DOI: 10.1063/5.0219431

centered peroxy radicals •OOOOOH. In low temperature combustion, the •OOOOOH radicals can undergo analogous intramolecular H-shift and dissociation to OH radical and ketohydroperoxide with subsequent thermal or prompt decomposition to additional radicals (chain branching). In the atmosphere, multiple cycles of hydrogen shift (ROO• to •QOOH) and O2 addition (•QOOH to •OOQOOH) can lead to autoxidation, ²⁸ producing more highly oxygenated and lower volatility organic molecules. ²⁹ Atmospheric oxidation of isoprene has been shown to proceed via a β-QOOH radical to yield epoxides (cyclic ethers), a precursor to secondary organic aerosol (SOA) formation. 30-32

The •QOOH intermediate is the 'central switchyard' in the chain reaction pathway, ²⁶ yet rarely observed, and requires further characterization for understanding the oxidation mechanism. Direct experimental observation of •QOOH radicals is extremely limited to date. Previously, a resonantly stabilized •QOOH derived from oxidation of 1,3-cycloheptadiene was identified using photoionization detection.³³ The resonance stabilization in this system enhanced the stability of the •OOOH radical and significantly raised the TS barrier for its unimolecular decomposition to OH products (about 30 kcal mol⁻¹), in contrast to the roughly three-fold lower barriers predicted for a wide range of •OOOH radicals.³⁴ This group recently achieved direct spectroscopic identification of a prototypical four-carbon •QOOH radical [•CH₂(CH₃)₂COOH] produced in isobutane oxidation with a barrier to unimolecular decay of only 10.3 kcal mol⁻¹. 35-37 The current focus is extension from acyclic to cyclic •QOOH radicals, in particular the six-carbon cyclic •QOOH transiently formed in cyclohexane oxidation.³⁸

The oxidation pathway of cyclohexane leads to three distinct carbon-centered hydroperoxycyclohexyl radicals (${}^{\bullet}C_6H_{10}OOH$), β -, γ -, and δ -QOOH, with α -QOOH predicted to be unstable. ³⁹ The three •QOOH isomers with radical positions at β -, γ -, and δ -carbon sites of the cyclohexyl ring have similar stabilities that differ from one another by only ca. 1 kcal mol⁻¹ relative to cyclohexyl + O₂. The primary pathways for unimolecular decay of the •QOOH radicals in cyclohexane oxidation are shown in Figure 1. The unimolecular decay pathways for β -, γ -, and δ -QOOH differ significantly from one another in the transition state (TS) barriers leading to hydroxyl (OH) radical and cyclohexylperoxy radical (ROO•) products. High-accuracy stationary point energies for the TS barriers were recently obtained utilizing a benchmarking approach, which was built on high-level reference calculations for the smaller ethane oxidation (C₂H₅O₂) system.³¹ For β-QOOH, the lowest energy decay pathway has a TS barrier of 9.49 kcal mol⁻¹, which involves simultaneous O-O bond elongation and C-O-O angle contraction to produce 1,2-epoxy-cyclohexane + OH products (see Figure S1). The H-atom transfer pathway from β-QOOH to the cyclohexylperoxy radical (ROO•) has a significantly higher TS barrier (18.5 kcal mol⁻¹) and is not expected to be competitive with the OH product formation pathway. The unimolecular decay pathways for γ - and δ -QOOH to OH products have notably higher TS barriers (ca. 17-19 kcal mol⁻¹) and

PLEASE CITE THIS ARTICLE AS DOI: 10.1063/5.0219431

similar or lower TS barriers to ROO• (13-18 kcal mol⁻¹), generally favoring ROO• products. Furthermore, with its deep well, the ROO• product effectively serves as a trap with no further immediate reaction.

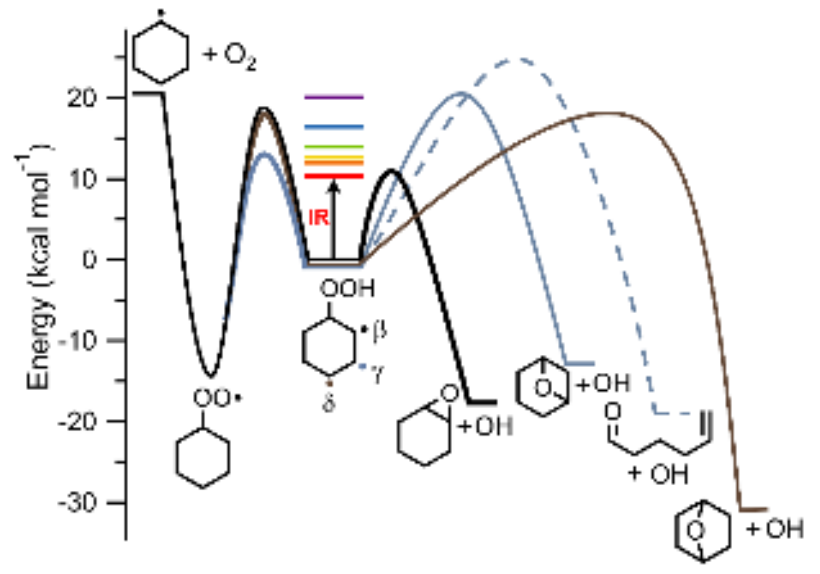


Figure 1. Energy profiles for unimolecular decay pathways of carbon-centered hydroperoxy cyclohexyl •QOOH radicals (• $C_6H_{10}OOH$) to OH + cyclic ethers (or hex-5-enal) or ROO• ($C_6H_{11}OO$ •) products. Three distinct •QOOH isomers (β -, γ -, and δ -QOOH) with similar stabilities (within 1 kcal mol⁻¹) can be formed with radical positions at different carbon sites of the cyclohexyl ring. The unimolecular decay pathways for β -, γ -, and δ -QOOH, shown with solid black, solid or dashed gray, and brown curves, respectively, differ considerably in the transition state (TS) barriers leading to OH and ROO• products. This study focuses on IR activation of β-QOOH, which is predicted to have near unity branching to OH + cyclic ether products over a wide range of energies (10-20 kcal mol⁻¹).

The present study focuses on the IR action spectrum of •QOOH intermediates formed in cyclohexane oxidation. The •QOOH intermediates are generated in the laboratory by H-atom abstraction from a cyclohexyl hydroperoxide (CHHP) precursor, ³⁸ and then jet-cooled in a supersonic expansion. The •OOOH radicals are vibrationally activated by IR excitation, which provides sufficient energy for •OOOH to surmount or tunnel through the TS barrier leading to OH radical and cyclic ether products. The OH products resulting from unimolecular decay are detected by UV laser-induced fluorescence (LIF). The resultant IR action spectrum spans from the fundamental OH stretch (v_{OH}, ca. 3600 cm⁻¹) to the overtone OH stretch (2_{VOH}, ca. 7000 cm⁻¹). Accompanying theoretical calculations utilizing second-order vibrational perturbation (VPT2) theory provide insight into the spectroscopic assignments of experimentally observed features. The isomer specificity of the observed IR transitions is further supported by recently predicted statistical unimolecular decay rates and branching ratios.³⁸ The spectral features of •QOOH are also compared with a corresponding IR transition of the CHHP precursor, and their time-resolved dissociation rates to OH products.

PLEASE CITE THIS ARTICLE AS DOI: 10.1063/5.0219431

Methods

The cyclic •QOOH radicals are generated by H-atom abstraction from a cyclohexyl hydroperoxide (CHHP) precursor. The newly formed •QOOH radicals are collisionally stabilized in the quartz capillary reactor tube and cooled to a rotational temperature of ca. 10 K in the supersonic jet expansion. CHHP has been prepared using a recently developed synthetic approach that avoids storage of large quantities of potentially explosive organic hydroperoxides, which is described in detail in Ref. 40. The vapor of the CHHP precursor is entrained in a gas mixture of Cl₂ (0.15%), He (15%), and Ar (85%) at 30 psig and pulsed through a solenoid valve with an affixed quartz capillary reactor tube (~25 mm length and 1 mm ID) into a vacuum chamber. Cl atoms are generated by photolyzing Cl₂ within the capillary tube using the third harmonic of a Nd:YAG laser (Continuum Precision 8000, ca. 4 mJ/pulse, 10 Hz). The Cl atoms can abstract an H-atom from different carbon sites of CHHP, resulting in three distinct hydroperoxylcyclohexyl radicals (β -, γ -, and δ -QOOH), as shown in Scheme 1. H-atom abstraction from the α ring site of CHHP leads to an unstable α -QOOH radical, ³⁹ which spontaneously decomposes to OH \pm cyclohexanone.

Scheme 1. Generation of •QOOH from the cyclohexyl hydroperoxide (CHHP) precursor. Cl atoms generated by 355 nm photolysis of Cl₂ abstract a H-atom from different carbon sites of CHHP to form •QOOH radicals.

The resultant •QOOH radicals are collisionally stabilized in the capillary tube and cooled to a rotational temperature of ca. 10 K upon supersonic expansion. Approximately 1 cm downstream, the counterpropagating and spatially overlapped IR-pump (ca. 9-26 mJ/pulse, 5 Hz) and UV-probe (ca. 1 mJ/pulse, 10 Hz) beams intersect the molecular beam in the collision free region. Tunable IR radiation is generated from a KTP-based OPO/OPA (Laservision; 0.9 cm⁻¹ bandwidth) pumped by a Nd:YAG laser (Continuum Surelite EX). The UV radiation is obtained from the frequency-doubled output of a Nd:YAG (EKSPLA NL300; 532 nm) pumped dye laser (ND6000, Rhodamine 590 dye). IR activation of •QOOH initiates unimolecular decay and generates the OH radical products that are detected by UV laser-induced fluorescence (LIF) on the $A^2\Sigma^+-X^2\Pi_{3/2}(1,0)$ $Q_1(3.5)$ transition at 282 nm. The resultant fluorescence on the OH $A^2\Sigma^+$ – $X^2\Pi_{3/2}(1,1)$ transition is detected. The IR action spectra of •QOOH are recorded with IR-UV time delays ranging from 40 to 400 ns, depending on the lifetime of vibrationally activated •OOOH. Active background subtraction (IR ON – IR OFF) is used to remove OH LIF signals that do not originate from IR activation. This background signal primarily arises from unimolecular decay of newly formed •QOOH radicals within the capillary tube, which are subsequently cooled in the supersonic expansion.

Chemical Physics

This is the author's peer reviewed, accepted manuscript. However, the online version of record will be different from this version once it has been copyedited and typeset

PLEASE CITE THIS ARTICLE AS DOI: 10.1063/5.0219431

Complementary electronic structure calculations are carried out at the B2PLYP-D3/cc-pVTZ level of theory using the Gaussian 16 software. The torsional landscape for •QOOH conformers and their harmonic frequencies are obtained employing the same theory/basis. Anharmonic vibrational frequencies and IR absorption intensities are calculated using second-order vibrational perturbation (VPT2) theory as implemented in Gaussian16. Note that the VPT2 calculations predict IR spectral features with one or two quanta of vibrational excitation; higher order excitation and couplings are not included. Initially, the electronic energy calculations for the cyclohexane oxidation (C₆H₁₁O₂) system were performed at CCSD(T)-F12/cc-pVTZ-F12//B2PLYP-D3/cc-pVTZ level. River the size and complexity of the cyclic C₆H₁₁O₂ system, applying a higher level of theory is impractical. Instead, a benchmarking approach using stationary point energies for the C₂H₅O₂ radical oxidation system was utilized to improve the accuracy of electronic energies for the C₆H₁₁O₂ system, as described in detail in our recent study.

Results

The experimental search to identify IR transitions of the hydroperoxy-cyclohexyl radical (•QOOH) is guided by calculated VPT2 anharmonic frequencies at the B2PLYP-D3/cc-pVTZ level of theory. The predicted IR transitions associated with the fundamental OH stretch (ν_{OH}) and overtone OH stretch (ν_{OH}) of the β -, γ -, and δ -QOOH isomers, including both axial and equatorial (dark and light color) conformers, are shown in Figure 2 (top three panels). In each case, the ν_{OH} transition is predicted at ca. 3600 cm⁻¹ with strong intrinsic intensity (ca. 30 km mol⁻¹), while the ν_{OH} transition predicted at ca. 7000 cm⁻¹ is ca. 5-fold weaker. The computed IR transitions for ν_{OH} -, ν_{OH} -, and ν_{OH} - are very similar to one another (Table S1), differing by only a few cm⁻¹.

The v_{OH} and $2v_{OH}$ regions of the experimental IR action spectrum of jet-cooled and stabilized •QOOH are shown in the bottom panel of Figure 2. Relative intensities of the experimental features are obtained from IR action spectroscopy as compared to absolute IR intensities reported for computed spectra. Moreover, IR action spectroscopy depends on both the IR absorption and the branching to the OH products, which together give rise to the UV LIF signal detected. The experimentally observed features at 3593.0 (red) and 7008.0 cm⁻¹ (purple) are attributed to the v_{OH} and $2v_{OH}$ transitions of •QOOH with frequencies and relative intensities similar to those predicted from VPT2 calculations. The experimental v_{OH} and $2v_{OH}$ features lie in between those predicted for the two conformers of β -QOOH, and both features are shifted to slightly lower frequency than those predicted for γ - or δ -QOOH. The similarity of predicted transitions for β , γ , δ -QOOH indicate that the experimentally observed IR features are not sufficient to definitively assign the isomer (or conformer) of •QOOH, given the accuracy of the theoretical predictions (ca. 10-20 cm⁻¹).

PLEASE CITE THIS ARTICLE AS DOI: 10.1063/5.0219431

AIP Publishing

3560 3600 7000 7040 Intensity 3560 7000 3600 7040 7000 3560 3800 7040 Expt. v_{OH} $2v_{OH}$ 0 7000 7040 3580 3800 Wavenumber (cm⁻¹)

Figure 2. Calculated anharmonic IR transitions in the fundamental OH stretch (ν_{OH}) and overtone OH stretch (ν_{OH}) regions for the axial and equatorial (dark and light color) conformers of the β-, γ-, and δ-QOOH isomers (top three panels), noting that the ν_{OH} transitions predicted for the axial and equatorial conformers of δ-QOOH are overlapped. The predicted IR transitions are shown using a Gaussian function to represent the typical breadth of the rotational band contour under jet-cooled conditions, ν_{Tot} color K. The experimentally observed ν_{OH} and ν_{OH} features (Expt., bottom panel) are obtained using IR action spectroscopy with UV laser-induced fluorescence detection of OH products.

Recently, this laboratory demonstrated that the β -QOOH isomer can be selectively identified based on its experimental appearance rate and branching ratio to OH products. The isomer selectivity originates from the distinctly different TS barriers associated with the β -, γ -, and δ -QOOH isomers, shown in Figure 1 (Table S2), and associated branching ratios to OH and ROO• products over the experimental energy range (3590 to 7010 cm⁻¹). The product branching ratios are derived from computed microcanonical decay rates in the prior study³⁸ and are shown in Figure 3. The TS barrier associated with β -QOOH dissociation to OH products (9.49 kcal mol⁻¹) is lower than that for its isomerization to ROO• (18.5 kcal mol⁻¹), resulting in near unity branching to OH products and negligible yield to ROO•. (Note that a minor channel from β -QOOH to HO₂ is also not significant.) By contrast, the TS barriers from γ - or δ -QOOH to OH products (ca. 17-19 kcal mol⁻¹) are higher than or comparable to those for isomerization to ROO• (ca. 13-18 kcal mol⁻¹) resulting in near unity branching to ROO• products for γ -QOOH or branching that shifts from ROO• to OH products with increasing energy for δ -QOOH.

The previously reported experimental unimolecular decay rates range from $4.6 \pm 1.6 \times 10^6 \text{ s}^{-1}$ (τ = 219 \pm 76 ns) at 3593.0 cm⁻¹ to \geq 2.8 \pm 0.5 \times 10⁸ s⁻¹ (τ \leq 3.6 \pm 0.6 ns laser-limited) at 7008.0 cm⁻¹ (Table S3).³⁸

PLEASE CITE THIS ARTICLE AS DOI: 10.1063/5.0219431

The experimental rates are in very good agreement with computed RRKM rates for unimolecular decay of β-QOOH to OH products, while they are much faster than those computed for the γ- and δ-QOOH isomers to OH products. Moreover, the computed unimolecular decay rates for δ-QOOH at energies with significant branching to OH products (6000-7000 cm⁻¹) are too slow (10⁴-10⁵ s⁻¹) for detection under the current experimental conditions. The computed RRKM rates and OH branching ratios for y-QOOH and δ-QOOH demonstrate that these isomers are not observed using infrared action spectroscopy. The present approach selectively detects β-QOOH and thereby differs from direct IR absorption spectroscopy, which would lack this isomer-specificity.

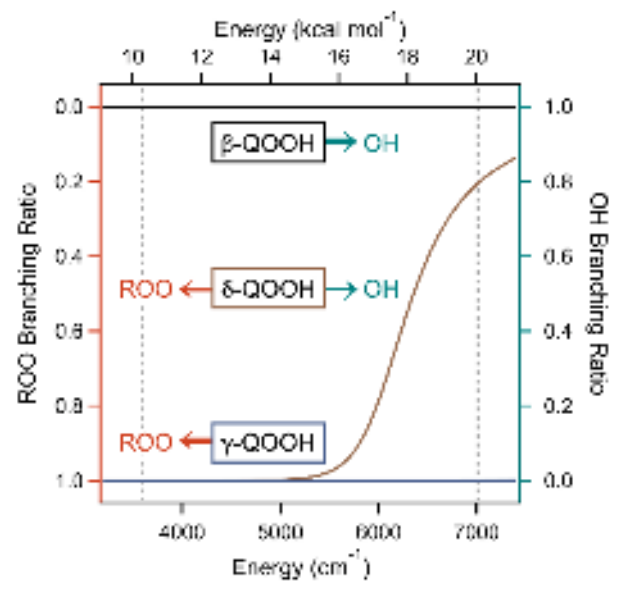


Figure 3. Branching ratios computed for β -, γ -, and δ -QOOH (black, blue, and gray traces) unimolecular dissociation pathways to OH (cyan) and ROO• (orange) product channels. The branching ratios are derived from the computed energy-dependent unimolecular decay rates using statistical RRKM theory. The vertical lines (dotted) represent the relevant energy range (ca. 3590 to 7010 cm⁻¹) of experiments. For β -QOOH the branching ratio is near unity to OH products, while for γ -QOOH the branching ratio is near unity to ROO• products. For δ-QOOH, the branching ratio shifts from favoring ROO• to OH with increasing energy, although the unimolecular decay rates for δ -OOOH are predicted to be much slower than observed experimentally.

Figure 4 shows an expanded view of the experimentally observed fundamental OH stretch of β-QOOH (v_{OH}) with rotational band contour of ca. 10 cm⁻¹ and a full width at half maximum (FWHM) of ca. 4 cm⁻¹. Rotational band contour simulations are performed with the PGOPHER program⁴² using computed rotational constants (A: 3.54 GHz, B: 1.57 GHz, and C: 1.30 GHz) and transition types (Table S4) obtained from the VPT2 calculation. A simulated band contour for a single vibrational transition with a rotational temperature of ca.10 K, IR OPO bandwidth (Gaussian) of 0.9 cm⁻¹, and homogeneous broadening (Lorentzian) of 1.7 cm⁻¹ agrees well with the experimental feature. The homogeneous broadening is primarily attributed to the rapid intramolecular vibrational redistribution (IVR) on a few

PLEASE CITE THIS ARTICLE AS DOI: 10.1063/5.0219431

picosecond timescale (ca. 3 ps), although some power broadening cannot be excluded. Here, IVR proceeds on a much faster timescale than the OH appearance rate, leading to statistical unimolecular decay of β -QOOH and observed rates independent of the initially excited vibrational modes.

 β -QOOH is predicted to have two conformers with axial (0 kcal mol⁻¹) and equatorial (0.4 kcal mol⁻¹) orientations of the hydroperoxide (–OOH) group relative to the cyclohexyl ring with only a ca. 4 kcal mol⁻¹ conformational barrier.¹⁹ The experimental spectrum exhibits a single ν_{OH} transition at 3593.0 cm⁻¹, which falls in between the predicted transitions for the axial (3587.8 cm⁻¹) and equatorial (3601.3 cm⁻¹) conformers of β -QOOH (Figure 2). The experimental observation of a single ν_{OH} feature indicates that the higher energy equatorial conformer is collisionally relaxed to the more stable axial conformer within the capillary and/or in the early stage of jet-expansion. The experimental spectrum in the 2 ν_{OH} region is also dominated by a single feature at 7008.0 cm⁻¹, which is again attributed to the more stable axial conformer of β -QOOH predicted at 7000.6 cm⁻¹. The corresponding simulated rotational band contour for the overtone OH stretch (2 ν_{OH} , 7008.0 cm⁻¹) of β -QOOH is shown in Figure S2.

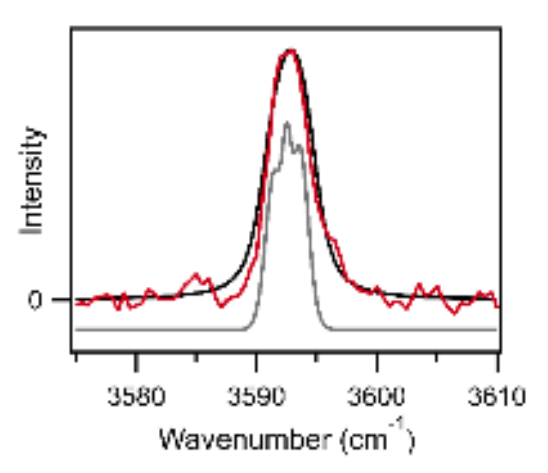


Figure 4. Expanded view of IR feature obtained for β-QOOH in the fundamental OH stretch (v_{OH} , 3593.0 cm⁻¹) region. The experimental spectrum (red) is simulated as a single vibrational band with a rotational temperature of ca. 10 K using rotational constants and transition type from the anharmonic VPT2 calculation for β-QOOH (Table S4). Simulations are shown at the IR OPO bandwidth (0.9 cm⁻¹, gray line) and with added contribution from homogenous broadening (1.7 cm⁻¹, black line) ascribed to rapid IVR (~3 ps), although some power broadening cannot be excluded.

Figure 5 shows a comprehensive experimental IR action spectrum of β -QOOH obtained in the spectral range between 3590 and 7010 cm⁻¹ with UV LIF detection of the OH products at various IR-UV time delays (40 to 400 ns, Table S5) and at a scan speed of 0.1 cm⁻¹/s. Asterisks in Figure 5 represent the observed features at which OH product appearance rates were measured in our prior study.³⁸ The IR–UV time delays utilized in different spectral regions are based on the experimental unimolecular decay rates (Table S3). The IR action spectrum of β -QOOH is displayed in two regions shown in top and bottom panels of Figure 5. The first region, ranging from 3560 to 4430 cm⁻¹, lies closer to the TS barrier (9.49

PLEASE CITE THIS ARTICLE AS DOI: 10.1063/5.0219431

kcal mol⁻¹), which includes the fundamental OH stretch (v_{OH}) and combination bands involving CH stretch and a lower-frequency mode ($v_{CH} + v_i$). The second region is recorded from 4840 to 7060 cm⁻¹ at energies significantly above the TS barrier, which covers features involving a combination of OH stretch and OOH bend $(v_{OH} + \delta_{OOH})$, overtone CH stretches $(2v_{CH})$, and overtone OH stretch $(2v_{OH})$. No significant features are predicted in the ca. 400 cm⁻¹ gap between the two regions. The OH LIF signal intensity of the observed IR features are normalized with OPO power. In addition, the intensities of the observed features are scaled to reflect the peak signal amplitude based on experimental OH product appearance and fall rates, as detailed in SI (Figure S3 and Table S3).

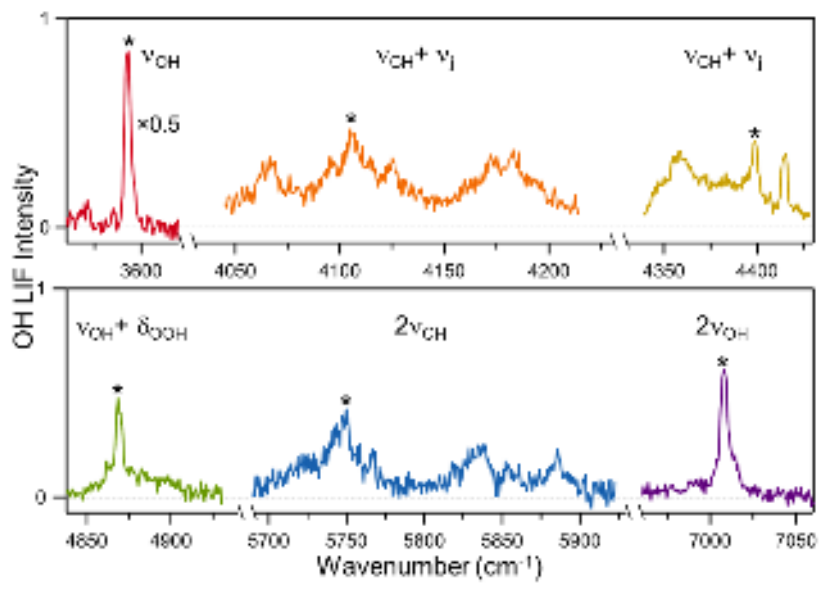


Figure 5. Experimental IR action spectrum for β-QOOH in the 3560 to 7060 cm⁻¹ region. The experimental IR action spectrum of β-QOOH is acquired by UV LIF detection of OH products at various IR-UV time delays (40 - 400 ns) determined by the energy-dependent β -QOOH dissociation rates. The OH LIF intensity scale is the same in top and bottom panels, except for the v_{OH} feature that is reduced by factor of 2. The intensity scale is relative OH LIF signal, which depends on both IR absorption and branching to OH products. The intensities are normalized to OPO power and scaled to reflect the peak signal amplitude (see SI). Asterisks indicate features at which experimental rate measurements have been performed.

Starting with the first region (Figure 5, top panel), the strongest feature in the experimental IR spectrum at 3593.0 cm⁻¹ (red), discussed earlier, is attributed to the fundamental OH stretch (v_{OH}) associated with the hydroperoxide (-OOH) group (Table S6). Several weaker transitions are observed in the 4050 to 4210 cm⁻¹ (orange) and 4340 to 4430 cm⁻¹ (yellow) spectral ranges. The experimental IR spectrum in the lower spectral range (orange) reveals three major features centered at ca. 4066, 4105, and 4183 cm⁻¹. In the higher energy region (yellow), the observed spectrum also exhibits three distinctive features peaked at 4340, 4398, and 4415 cm⁻¹. Most of these observed features are broad and unstructured, suggesting that they are composed of many overlapping transitions. In addition, the

PLEASE CITE THIS ARTICLE AS DOI: 10.1063/5.0219431

Figure 6 (top panel) shows the computed IR spectrum for β-QOOH, starting from the fundamental OH stretch and continuing through multiple IR transitions predicted in the 3900 to 4500 cm⁻¹ range, the latter primarily involving combination bands of fundamental CH stretches and a lower-frequency mode ($v_{CH} + v_j$). The CH stretches involve five distinct -CH₂ groups and a •CH radical center, which give rise to a cluster of fundamental CH stretches of the -CH₂ groups (v_{CH_2}) in the 2800-3000 cm⁻¹ region (Table S7) and the CH stretch (v_{CH}) of the unique •CH radical site at higher frequency (3074 cm⁻¹). The lower-frequency modes (v_j) likely involve HCH bend ($v_{CH} + v_{CH_2} + v_{CH_2$

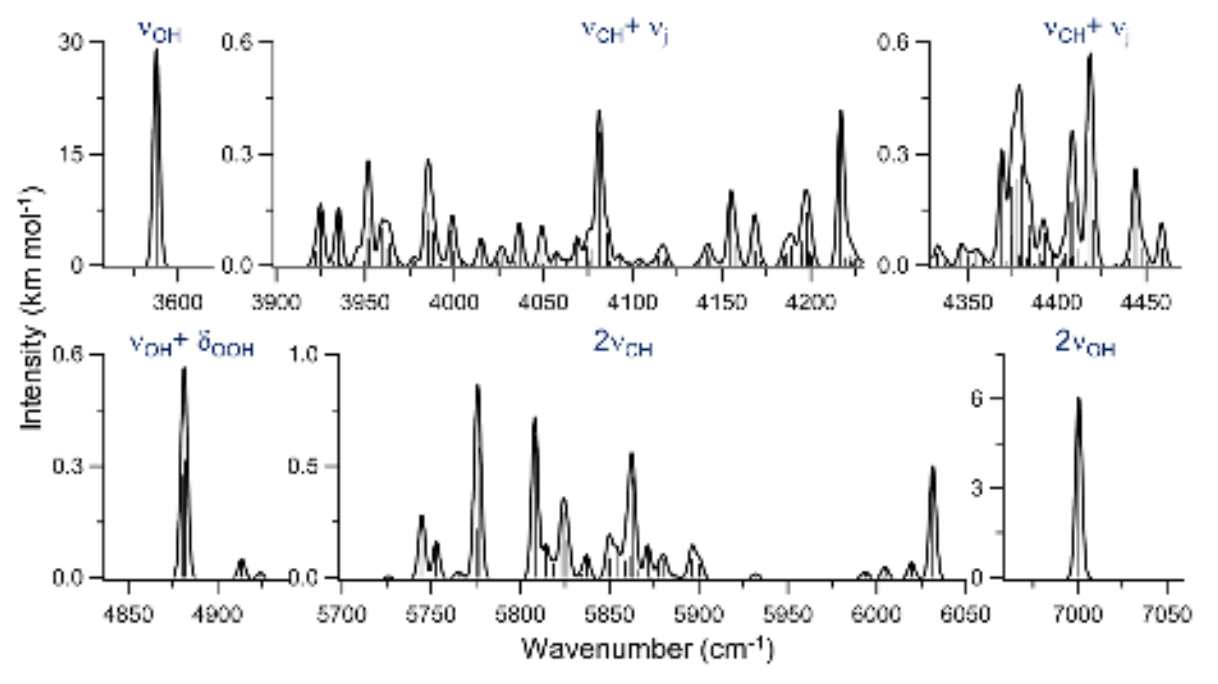


Figure 6. Anharmonic frequencies and intrinsic intensities of IR transitions predicted for the axial conformer of β-QOOH in the 3560 to 7060 cm⁻¹ region based on VPT2 calculations. The spectral range includes the fundamental OH stretch (ν_{OH}), combination bands involving CH stretch and low-frequency modes ($\nu_{CH} + \nu_j$), a combination band of OH stretch and OOH bend ($\nu_{OH} + \delta_{OOH}$), overtone CH stretches (ν_{CH}), and the overtone OH stretch (ν_{CH}). The calculated transitions (sticks) are convoluted with a Gaussian function to represent the breadth of rotational band contours under jet-cooled conditions ($\nu_{CH} + \nu_{CH}$). Note that the intensity scales of panels change in different spectral regions.

PLEASE CITE THIS ARTICLE AS DOI: 10.1063/5.0219431

Moving to higher excitation energies (Figure 5), the experimental spectrum exhibits a distinct feature at 4868.5 cm⁻¹ (green), which is attributed to a combination band of OH stretch and OOH bend (v_{OH} + δ_{OOH}) associated with the -OOH group predicted at 4881.8 cm⁻¹ (Figure 6, bottom panel). This experimental feature is surprisingly stronger than predicted theoretically. A prior study of the •QOOH intermediate in isobutane oxidation also revealed a greater intensity for the v_{OH} + δ_{OOH} feature compared to that predicted by VPT2 calculations.³⁶ The enhanced intensity was attributed to couplings between the OH stretch and/or OOH bend and the OO stretch.

Figure 6 (bottom panel) also shows multiple overtone CH stretches (e.g. 2v₂) and combinations of two different CH stretches (e.g. $v_2 + v_3$) involving -CH₂ groups (denoted $2v_{CH}$) predicted as a cluster of transitions in the 5700-5950 cm⁻¹ region. Figure 5 reveals three distinctive features (5750, 5838, and 5885 cm⁻¹) observed in the experimental scan from 5690 to 5920 cm⁻¹ (blue). However, the overtone CH stretch associated with the •CH radical site of β-OOOH predicted at 6031 cm⁻¹ was not observed in a spectral search of the 5975-6050 cm⁻¹ region (not shown), suggesting that this transition is weaker than predicted.

Finally, the characteristic band associated with the overtone OH stretch (2v_{OH}) of β-QOOH, discussed earlier, is observed at 7008.0 cm⁻¹ (purple trace, Figure 5). Closer examination of the experimental 2v_{OH} feature reveals a shoulder on the higher wavenumber side, as shown in Figure S2. The shoulder is unlikely to originate from the equatorial conformer, which is predicted to occur ca. 15 cm⁻¹ higher (Figure 2, Table S1). However, conformers associated with torsional isomerization pathways, such as CCOO and COOH motions, can have closely spaced 2v_{OH} transitions as observed previously for •QOOH in isobutane oxidation.³⁶ This suggests that the observed shoulder may also originate from conformers associated with torsional motions.

In a recent study, the $2v_{OH}$ transition of the CHHP precursor was observed at 7012.5 cm⁻¹ (FWHM ~ ca. 7.5 cm⁻¹) using an IR multiphoton dissociation method with UV LIF detection of resulting OH products. 40 The observed 2v_{OH} feature of β-OOOH at 7008.0 cm⁻¹ (FWHM ~ ca. 4.0 cm⁻¹) is shifted from the CHHP feature by only 4.5 cm⁻¹ (Figure S5, Table S8). Nevertheless, the present experimental approach readily distinguishes between IR transitions of β-QOOH and the CHHP precursor. Figure 7 shows the comparison of temporal appearance profiles for OH products upon 2voH excitation of CHHP and β -QOOH. The appearance of OH products upon unimolecular decay of β -QOOH (2 ν _{OH}) occurs rapidly (≤ 3.6 ns), while OH products from IR multiphoton dissociation of CHHP ($2v_{OH}$) are released orders of magnitude more slowly (≥ 1500 ns).⁴⁰ As a result, a short IR–UV time delay (40 ns) strongly favors detection of β-QOOH over the CHHP precursor. In addition, the IR multiphoton spectrum of CHHP can be recorded in pure Ar carrier gas. 40 and is unchanged upon 355 nm photolysis and/or addition

PLEASE CITE THIS ARTICLE AS DOI: 10.1063/5.0219431

of Cl₂ to the carrier gas. In contrast, observation of β-QOOH requires 355 nm photolysis of Cl₂ added to the carrier gas mixture. Finally, the IR power dependencies for 2v_{OH} features of CHHP and β-QOOH are shown in Figure S6. The nonlinear IR power dependence for CHHP indicates multiphoton absorption, while the linear IR power dependence for β -QOOH confirms its linear absorption. Notably, under optimized experimental conditions for generating and observing β-QOOH, essentially no signal is detected for CHHP.

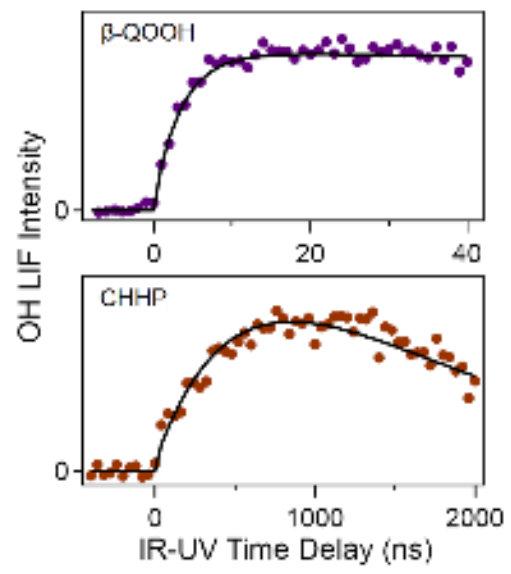


Figure 7. Time profiles for OH products upon excitation of β-OOOH and CHHP in the overtone OH stretch (2v_{OH}) region. Temporal profiles are shown for appearance of OH products resulting from IR activation of β-QOOH at 7008.0 cm⁻¹ (purple, top) and IR multiphoton excitation of CHHP at 7012.5 cm⁻¹ (gray, bottom). Fits of the OH appearance profiles yield lifetimes of $\leq 3.6 \pm 0.6$ ns for β -QOOH and \geq 1500 ns for CHHP. The top panel is adapted from Ref. ³⁸ and the bottom panel is obtained from Ref. ⁴⁰.

Conclusion

Hydroperoxy-cyclohexyl radicals (•QOOH) transiently formed in cyclohexane oxidation have been stabilized, jet-cooled, and characterized through their IR action spectrum using LIF detection of OH products. The cyclohexane oxidation pathway leads to three nearly degenerate carbon-centered hydroperoxy-cyclohexyl isomers, β -, γ -, and δ -QOOH, which are generated in the laboratory by H-atom abstraction from corresponding ring sites of the cyclohexyl hydroperoxide precursor. The three isomers are predicted to have similar fundamental and overtone OH stretch transitions, which differ from one another by only a few cm⁻¹ in each spectral region, precluding definitive identification by IR spectroscopy alone. Instead, β-QOOH is identified as the spectral carrier with additional insight from its near-unity branching ratio and rapid unimolecular decay rate to OH products.

IR spectral features of β-QOOH have been selectively observed in the 3590-7010 cm⁻¹ range (ca. 10-20 kcal mol⁻¹) at energies in the vicinity of the TS barrier (9.49 kcal mol⁻¹) leading to OH products. The

PLEASE CITE THIS ARTICLE AS DOI: 10.1063/5.021943

spectral range encompasses fundamental and overtone OH stretch transitions, overtone CH stretch transitions, and combination bands involving OH or CH stretch and lower frequency modes. Assignment of the IR spectral features is guided by the theoretically predicted (VPT2) IR absorption spectrum for β-QOOH. The identification of a single vibrational band for the fundamental OH stretch of β -QOOH (ν_{OH}), at 3593.0 cm⁻¹, simulated at a rotational temperature of 10 K, is also indicative of efficient equatorial-toaxial conformational relaxation. Finally, the overtone OH stretch ($2v_{OH}$) of β -QOOH at 7008.0 cm⁻¹ is further distinguished from the corresponding transition of the cyclohexyl hydroperoxide precursor (7012.5 cm⁻¹) by the prompt vs. slow OH product appearance rates and linear vs. quadratic IR power dependencies. The experimental and theoretical IR fingerprint for the β-QOOH radical, along with theoretical predictions for γ - and δ -QOOH, provide a guide for detection of these elusive intermediates under realistic atmospheric and/or combustion conditions.

Conflicts of interest

There are no conflicts to declare.

Data availability

All supporting data are available in the Supporting Information.

Supplementary Material

The Supporting Material provides additional details on experimental and theoretical methods; fits to rotational band contours; simulated temporal profiles; experimental and computed IR spectra; power dependencies; unimolecular decay rates; and descriptions of the calculated frequencies.

Acknowledgments

Research in the Lester laboratory was supported by the US Department of Energy, Office of Science, Basic Energy Sciences under grant DE-FG02-87ER13792. Work at Argonne National Laboratory was supported by the US Department of Energy, Office of Science, Basic Energy Sciences, Division of Chemical Sciences, Geosciences, and Biosciences under contract No. DE-AC02-06CH11357. M.C.K. is grateful to the NSF (CHE-2102626) for financial support of this research. Partial instrumentation support (NMR spectrometer) was provided by NSF CHE-1827457 and the Vagelos Institute for Energy Science and Technology. T.K.R. was primarily supported by a Walter-Benjamin Scholarship funded by the Deutsche Forschungsgemeinschaft (DFG, German Research Foundation) - Project number 508074809. This work used the Advanced Cyberinfrastructure Coordination Ecosystem: Service & Support (ACCESS) program, which is supported by National Science Foundation grants #2138259, #2138286, #2138307, #2137603, and #2138296, through the allocation TG-CHE190088.

the online version of record will be different from this version once it has been copyedited and typeset

PLEASE CITE THIS ARTICLE AS DOI: 10.1063/5.021943

This is the author's peer reviewed, accepted manuscript. However,

AIP Publishing

References

- ¹ S. M. Sarathy; G. Kukkadapu; M. Mehl; T. Javed; A. Ahmed; N. Naser; A. Tekawade; G. Kosiba; M. AlAbbad; E. Singh; et al. "Compositional effects on the ignition of FACE gasolines," *Combust. Flame* **169**, 171-193 (2016).
- ² S. Dooley; S. H. Won; M. Chaos; J. Heyne; Y. Ju; F. L. Dryer; K. Kumar; C.-J. Sung; H. Wang; M. A. Oehlschlaeger; et al. "A jet fuel surrogate formulated by real fuel properties," *Combust. Flame* **157**, 2333-2339 (2010).
- ³ W. J. Pitz; C. J. Mueller. "Recent progress in the development of diesel surrogate fuels," *Progr. Energy Combust. Sci.* **37**, 330-350 (2011).
- ⁴ L. M. Balster; E. Corporan; M. J. DeWitt; J. T. Edwards; J. S. Ervin; J. L. Graham; S.-Y. Lee; S. Pal; D. K. Phelps; L. R. Rudnick; et al. "Development of an advanced, thermally stable, coal-based jet fuel," *Fuel Process. Technol.* **89**, 364-378 (2008).
- ⁵ R. Sommariva; R. S. Blake; R. J. Cuss; R. L. Cordell; J. F. Harrington; I. R. White; P. S. Monks. "Observations of the Release of Non-methane Hydrocarbons from Fractured Shale," *Environ. Sci. Technol.* **48**, 8891-8896 (2014).
- ⁶ S. J. Eaton; S. H. Beis; S. A. Karunarathne; H. P. Pendse; M. C. Wheeler. "Hydroprocessing of biorenewable thermal deoxygenation oils," *Energy Fuels* **29**, 3224-3232 (2015).
- ⁷ Y. Yang; A. L. Boehman; J. M. Simmie. "Uniqueness in the low temperature oxidation of cycloalkanes," *Combust. Flame* **157**, 2357-2368 (2010).
- ⁸ A. Landera; R. P. Bambha; N. Hao; S. P. Desai; C. M. Moore; A. D. Sutton; A. George. "Building Structure-Property Relationships of Cycloalkanes in Support of Their Use in Sustainable Aviation Fuels," *Front. Energy Res.* **9**, 771697 (2022).
- ⁹ Y. B. Lim; P. J. Ziemann. "Effects of Molecular Structure on Aerosol Yields from OH Radical-Initiated Reactions of Linear, Branched, and Cyclic Alkanes in the Presence of NO_x," *Environ. Sci. Technol.* **43**, 2328-2334 (2009).
- ¹⁰ J. F. Hunter; A. J. Carrasquillo; K. E. Daumit; J. H. Kroll. "Secondary Organic Aerosol Formation from Acyclic, Monocyclic, and Polycyclic Alkanes," *Environ. Sci. Technol.* **48**, 10227-10234 (2014).
- ¹¹ L. G. Jahn; D. S. Wang; S. V. Dhulipala; L. H. Ruiz. "Gas-Phase Chlorine Radical Oxidation of Alkanes: Effects of Structural Branching, NO_x, and Relative Humidity Observed during Environmental Chamber Experiments," *J. Phys. Chem. A* **125**, 7303-7317 (2021).
- ¹² Y. Zhao; N. T. Nguyen; A. A. Presto; C. J. Hennigan; A. A. May; A. L. Robinson. "Intermediate Volatility Organic Compound Emissions from On-Road Gasoline Vehicles and Small Off-Road Gasoline Engines," *Environ. Sci. Technol.* **50**, 4554-4563 (2016).
- ¹³ W. Hu; H. Zhou; W. Chen; Y. Ye; T. Pan; Y. Wang; W. Song; H. Zhang; W. Deng; M. Zhu; et al. "Oxidation Flow Reactor Results in a Chinese Megacity Emphasize the Important Contribution of S/IVOCs to Ambient SOA Formation," *Environ. Sci. Technol.* **56**, 6880-6893 (2022).
- ¹⁴ T. Chatterjee; M. Wang; S. W. Wagnon; G. Kukkadapu; C.-J. Sung; W. J. Pitz. "Autoignition of cyclohexane at low-to-intermediate temperatures: Rapid compression machine experiments and improved comprehensive chemical kinetic model," *Combust. Flame* **259**, 113187, and referenced cited therein (2024).
- ¹⁵ S. M. Aschmann; J. Arey; R. Atkinson. "Reactions of OH Radicals with C₆−C₁₀ Cycloalkanes in the Presence of NO: Isomerization of C₇−C₁₀ Cycloalkoxy Radicals," *J. Phys. Chem. A* **115**, 14452-14461 (2011).
- ¹⁶ J. Platz; J. Sehested; O. J. Nielsen; T. J. Wallington. "Atmospheric Chemistry of Cyclohexane: UV Spectra of c-C₆H₁₁ and (c-C₆H₁₁)O₂ Radicals, Kinetics of the Reactions of (c-C₆H₁₁)O₂ Radicals with NO and NO₂, and the Fate of the Alkoxy Radical (c-C₆H₁₁)O," *J. Phys. Chem. A* **103**, 2688-2695 (1999).
- ¹⁷ Z. Serinyel; O. Herbinet; O. Frottier; P. Dirrenberger; V. Warth; P. A. Glaude; F. Battin-Leclerc. "An experimental and modeling study of the low- and high-temperature oxidation of cyclohexane," *Combust. Flame* **160**, 2319-2332 (2013).

the online version of record will be different from this version once it has been copyedited and typeset

PLEASE CITE THIS ARTICLE AS DOI: 10.1063/5.021943

This is the author's peer reviewed, accepted manuscript. However,

- ¹⁸ R. X. Fernandes; J. Zádor; L. E. Jusinski; J. A. Miller; C. A. Taatjes. "Formally direct pathways and low-temperature chain branching in hydrocarbon autoignition: the cyclohexyl + O₂ reaction at high pressure," Phys. Chem. Chem. Phys. 11, 1320-1327 (2009).
- ¹⁹ A. M. Knepp; G. Meloni; L. E. Jusinski; C. A. Taatjes; C. Cavallotti; S. J. Klippenstein. "Theory, measurements, and modeling of OH and HO₂ formation in the reaction of cyclohexyl radicals with O₂," Phys. Chem. Chem. Phys. 9, 4315-4331 (2007).
- ²⁰ J. Bourgalais; H.-H. Carstensen; O. Herbinet; G. A. Garcia; P. Arnoux; L.-S. Tran; G. Vanhove; L. Nahon; M. Hochlaf; F. Battin-Leclerc. "Product identification in the low-temperature oxidation of cyclohexane using a jet-stirred reactor in combination with SVUV-PEPICO analysis and theoretical quantum calculations," J. Phys. Chem. A 126, 5784-5799 (2022).
- ²¹ C. Cavallotti; R. Rota; T. Faravelli; E. Ranzi, "Ab initio evaluation of primary cyclo-hexane oxidation reaction rates," *Proc. Combust. Inst.* **31**, 201-209 (2007).
- ²² B. Sirjean; P. A. Glaude; M. F. Ruiz-Lòpez; R. Fournet. "Theoretical kinetic study of the reactions of cycloalkylperoxy radicals," J. Phys. Chem. A 113, 6924-6935 (2009).
- ²³ J. Zou: Y. Li: L. Ye: H. Jin. "A comprehensive study on low-temperature oxidation chemistry of cyclohexane. I. Conformational analysis and theoretical study of first and second oxygen addition," Combust. Flame 235, 111658 (2022).
- ²⁴ J. Zou; H. Jin; D. Liu; X. Zhang; H. Su; J. Yang; A. Farooq; Y. Li. "A comprehensive study on lowtemperature oxidation chemistry of cyclohexane. II. Experimental and kinetic modeling investigation," Combust. Flame 235, 111550 (2022).
- ²⁵ J. Zádor; C. A. Taatjes; R. X. Fernandes. "Kinetics of elementary reactions in low-temperature autoignition chemistry," *Prog. Energy Combust. Sci.* **37**, 371-421 (2011).
- ²⁶ D. L. Osborn. "Reaction mechanisms on multiwell potential energy surfaces in combustion (and atmospheric) chemistry," Annu. Rev. Phys. Chem. 68, 233-260 (2017).
- ²⁷ J. J. Orlando; G. S. Tyndall, "Laboratory studies of organic peroxy radical chemistry: an overview with emphasis on recent issues of atmospheric significance," Chem. Soc. Rev. 41, 6294-6317 (2012).
- ²⁸ J. D. Crounse; L. B. Nielsen; S. Jørgensen; H. G. Kjaergaard; P. O. Wennberg. "Autoxidation of Organic Compounds in the Atmosphere," J. Phys. Chem. Lett. 4, 3513-3520 (2013).
- ²⁹ M. Rissanen. "Anthropogenic Volatile Organic Compound (AVOC) Autoxidation as a Source of Highly Oxygenated Organic Molecules (HOM)," J. Phys. Chem. A 125, 9027-9039 (2021).
- ³⁰ F. Paulot; J. D. Crounse; H. G. Kjaergaard; A. Kürten; J. M. St. Clair; J. H. Seinfeld; P. O. Wennberg. "Unexpected epoxide formation in the gas-phase photooxidation of isoprene," Science 325, 730-733 (2009).
- ³¹ E. L. D'Ambro; S. Schobesberger; C. J. Gaston; F. D. Lopez-Hilfiker; B. H. Lee; J. Liu; A. Zelenvuk; D. Bell; C. D. Cappa; T. Helgestad; et al. "Chamber-based insights into the factors controlling epoxydiol (IEPOX) secondary organic aerosol (SOA) yield, composition, and volatility," Atmos. Chem. Phys. 19, 11253-11265 (2019).
- ³² K. H. Møller; T. Kurtén; K. H. Bates; J. A. Thornton; H. G. Kjaergaard. "Thermalized epoxide formation in the atmosphere," J. Phys. Chem. A 123, 10620-10630 (2019).
- ³³ J. D. Savee; E. Papajak; B. Rotavera; H. Huang; A. J. Eskola; O. Welz; L. Sheps; C. A. Taatjes; J. Zádor; D. L. Osborn, "Direct observation and kinetics of a hydroperoxyalkyl radical (OOOH)," Science **347**, 643-646 (2015).
- ³⁴ J. Bugler; J. Power; H. J. Curran. "A theoretical study of cyclic ether formation reactions," *Proc.* Combust. Inst. 36, 161-167 (2017).
- ³⁵ A. S. Hansen; T. Bhagde; K. B. Moore; D. R. Moberg; A. W. Jasper; Y. Georgievskii; M. F. Vansco; S. J. Klippenstein; M. I. Lester. "Watching a hydroperoxyalkyl radical (•QOOH) dissociate," Science 373, 679-682 (2021).
- ³⁶ A. S. Hansen; T. Bhagde; Y. Qian; A. Cavazos; R. M. Huchmala; M. A. Boyer; C. F. Gavin-Hanner; S. J. Klippenstein; A. B. McCov; M. I. Lester. "Infrared spectroscopic signature of a hydroperoxyalkyl radical (•QOOH)," J. Chem. Phys. 156, 014301 (2022).

PLEASE CITE THIS ARTICLE AS DOI: 10.1063/5.0219431

- ³⁷ T. Bhagde; A. S. Hansen; S. Chen; P. J. Walsh; S. J. Klippenstein; M. I. Lester. "Energy-resolved and time-dependent unimolecular dissociation of hydroperoxyalkyl radicals (•OOOH)," Faraday Discuss. **238**, 575-588 (2022).
- ³⁸ Y. Qian; T. K. Roy; A. W. Jasper; C. A. Sojdak; M. C. Kozlowski; S. J. Klippenstein; M. I. Lester. "Isomer-resolved unimolecular dynamics of the hydroperoxyalkyl intermediate (•QOOH) in cyclohexane oxidation," Proc. Natl. Acad. Sci. U.S.A. 121, e2401148121 (2024).
- ³⁹ J. M. Anglada; R. Crehuet; J. S. Francisco. "The stability of α-hydroperoxyalkyl radicals," *Chem. Eur. J.* **22**, 18092-18100 (2016).
- ⁴⁰ T. K. Roy; Y. Qian; E. Karlsson; R. Rabayah; C. A. Sojdak; M. C. Kozlowski; T. N. V. Karsili; M. I. Lester. "Vibrational spectroscopy and dissociation dynamics of cyclohexyl hydroperoxide," *Chem. Sci.* **15**, 6160-6167 (2024).
- ⁴¹ M. J. Frisch; G. W. Trucks; H. B. Schlegel; G. E. Scuseria; M. A. Robb; J. R. Cheeseman; G. Scalmani; V. Barone; G. A. Petersson; H. Nakatsuji. and et al., Gaussian 16, Rev. C.01; Gaussian, Inc.: Wallingford, CT, 2016.
- ⁴² C. M. Western. "PGOPHER: A program for simulating rotational, vibrational and electronic spectra," J. *Quant. Spectrosc. Radiat. Transfer* **186**, 221-242 (2017).